Title

The electrochemical behavior of poly 1-pyrenemethyl methacrylate binder and its effect on the interfacial chemistry of a silicon electrode

Permalink

https://escholarship.org/uc/item/5sm8g5fp

Authors

Haregewoin, Atetegeb Meazah
Terborg, Lydia
Zhang, Liang
et al.

Peer reviewed

The electrochemical behavior of poly 1-pyrenemethyl methacrylate binder and its effect on the interfacial chemistry of a silicon electrode

Atetegeb Meazah Haregewoin[a], Lydia Terborg[a,1], Liang Zhang[b], Sunhyung Jurng[c], Brett L. Lucht[c], Jinghua Guo[b], Philip N. Ross[a], Robert Kostecki[a,*]

[a] Energy Storage & Distributed Resources Division, Lawrence Berkeley National Laboratory, One Cyclotron Road, Berkeley, CA 94720, USA
[b] Advanced Light Source, Lawrence Berkeley National Laboratory, One Cyclotron Road, Berkeley, CA 94720, USA
[c] Department of Chemistry, University of Rhode Island, Kingston, RI 02881, USA

HIGHLIGHTS

- PPy binder shows improved adhesion to Si and Cu with regard to PVdF and PAALi.
- PPy thin film alters electrochemical response of the Si electrode.
- Mechanical and interfacial properties of Si electrode depend on PPy binder topology.

ARTICLE INFO

ABSTRACT

The physico-chemical properties of poly (1-pyrenemethyl methacrylate) (PPy) are presented with respect to its use as a binder in a Si composite anode for Li-ion batteries. PPy thin-films on Si(100) wafer and Cu model electrodes are shown to exhibit superior adhesion as compared to conventional polyvinylidene difluoride (PVdF) binder. Electrochemical testing of the model bi-layer PPy/Si(100) electrodes in a standard organic carbonate electrolyte reveal higher electrolyte reduction current and an overall irreversible cathodic charge consumption during initial cycling versus the uncoated Si electrode. The PPy thin-film is also shown to impede lithiation of the underlying Si. XAS, AFM, TGA and ATR-FTIR analysis indicated that PPy binder is both chemically and electrochemically stable in the cycling potential range however significant swelling is observed due to a selective uptake of diethyl carbonate (DEC) from the electrolyte. The increased concentration of DEC and depletion of ethylene carbonate (EC) at the Si/PPy interface leads to continuous decomposition of the electrolyte and results in non-passivating behavior of the Si(100)/PPy electrode as compared to pristine silicon. Consequently, PPy binder improves the mechanical integrity of composite Si anodes but it influences mass transport at the Si(100)/PPy interface and alters electrochemical response of silicon during cycling in an adverse manner.

1. Introduction

The development of intermetallic anode materials such as Si, Sn, Sb is being pursued to improve the power and energy densities of commercial Li-ion batteries. Silicon has high volumetric energy density (972 Wh L^{-1}) compared to the widely used carbon-based electrodes (253 Wh L^{-1}), which makes it a promising candidate to replace graphite electrodes [1,2]. However, previous studies have suggested that there is inherently non-passivating behavior of silicon in standard Li-ion electrolytes [3–5] that is aggravated by significant volume changes (~320%) of silicon during the charging and discharging processes.

Mechanical stresses from volume change lead to particle decrepitation, resulting in electronic isolation of particles, loss of mechanical integrity of composite electrodes and interfacial instability. Particle factures expose fresh Si surface to the electrolyte during cycling, leading to formation of a thick film of electrolyte reduction products, causing impedance rise, capacity loss and lithium inventory shift in the cell [5,6].

One approach to overcome the loss of electronic connectivity and mechanical integrity in the composite Si electrode during extended charge-discharge cycles is to use an effective binder. Strong adhesion to the electrode's active (e.g., Si, graphite) and passive (e.g., Cu current

collector, carbon conductive additive) components, high tensile strength and low Young's modulus are just a few desirable mechanical properties of such binder materials. Poly (vinylidene fluoride) (PVdF) is the most commonly used binder in commercial Li-ion batteries. However, Si-based composite electrodes with PVdF binder show poor electrochemical performance *i.e.*, rapid capacity loss and impedance rise upon cycling [7,8]. Sodium carboxy-methyl cellulose (CMC) binder showed a significant improvement in capacity retention of Si anodes by producing strong bonds and links between the conductive carbon additive and Si particles [9]. Similarly, poly (acrylic acid) (PAA) binder has also been shown to improve the performance of composite Si electrodes [10]. Recently, Nguyen et al. reported that Si with PAA and Si with mixture of PAA and CMC electrodes have slightly better capacity retention than the Si with CMC but greatly outperformed Si with PVDF electrodes [11]. The authors showed that the improved performance in PAA and CMC is due to the presence of carboxylic and hydroxyl functional groups, that protects the surface from continuous reactions with the carbonate solvents. Their result suggests that besides improved mechanical properties these binders also influence reactions with the electrolyte and interfacial stability of the electrode.

Recently, new advanced polymer binders have attracted a lot of attention due to their claimed dual functionality as conductive additive that enhances the electrical connectivity between the active material particles, and improved adhesion to keep composite electrode mechanical integrity [12–16]. Ling et al. showed that the Si/C composite electrode with poly (1-pyrenemethyl methacrylate) (PPy) binder has a better cycling performance by increasing the utilization of Si than the Si/C with lithium polyacrylate (PAALi) binder [12]. Park et al. reported pyrene-based polymeric binders to improve the performance of Si anode [15]. The authors showed the conductive mechanism of the pyrene-based binder by measuring the electron mobility [15] and by integrating the electrochemical response of the polymer [12].

The improved electronic properties of bifunctional polymers also imply that such conductive binders could exhibit unique electrochemical activity toward the electrolyte and possibly alter interfacial properties of the Si composite electrode. Therefore, it is essential to study the fundamental mechanical and electrochemical properties of multifunctional binders to understand their role in composite Si-based negative electrodes during long-term cycling. This model study attempts to not only determine the nature and mechanism of PPy interactions in composite Si electrodes but also offer unique insights into rational design principles of advanced multifunctional binders for intermetallic Li-ion anodes.

2. Experimental

2.1. Chemicals

Lithium Poly (acrylic acid) (PAA, M_w = 450,000) and polyvinylidene difluoride (PVdF, M_w = 534,000) were purchased from Sigma-Aldrich and used as received. Poly (1-pyrenemethyl metacrylate (PPy, M_w = 34,000) was synthesized at Cell Analysis, Modeling and Prototyping (CAMP) facility at Argonne National Laboratory and kindly provided for testing in this work. Ethylene carbonate (EC, 99%, Sigma-Aldrich), diethyl carbonate (DEC, ≥ 99%, Sigma-Aldrich), fluoroethylene carbonate (FEC, ≥ 99%, Solvay), and lithium hexafluorophospate (LiPF$_6$, (≥99.99%, Sigma-Aldrich) were used to prepare 1.2 M LiPF$_6$, EC:DEC:FEC (2.1:4.9:3.0 v/v electrolyte solution. Dimethyl carbonate (DMC, ≥ 99%, Sigma-Aldrich) was used as the rinsing solvent.

2.2. Model electrode/cell preparation

The 500 μm thick B-doped p-type Si(100) wafers with 0.001 Ω-cm resistivity were purchased from MTI. Some Si(100) wafers were coated via e-beam evaporation with 100 nm Cu layer on top of 3 nm Cr

adhesion sublayer. Both Si(100) and Si(100)/Cu wafers were spin-coated with, 2 ml solution of 0.25 wt% PPy in chloroform at 3000 rpm for 60 s using P-6000 Spin Coater. To evaluate the thickness of the PPy film, the spin coated polymer film was removed with a razor blade and step height was imaged and profiled via atomic force microscopy (AFM, Agilent 5500 microscope). AFM micrographs (not shown here) revealed that the PPy film was ca. 25 ± 5 nm thick, and micrographs of the PPy surface showed it to be uniform with no observation of pin holes. The 25 nm thick film of PPy on the Si(100) and Si(100)/Cu electrodes closely resembles the estimated thickness of PPy coverage of silicon particles in Si/PPy (2:1) composite electrodes by Park et al. where uniform coverage was assumed [15]. The pristine Si(100) and PPy-coated wafers were cut to 1 × 1 cm squares, dried overnight under ambient conditions and further processed at 120 °C for 15 h under vacuum.

2.3. Electrochemical testing

Cyclic voltammetry (CV) measurements were performed at a scan rate of 0.1 mV s^{-1} using a VMP3 multichannel potentiostat (Bio-Logic Science Instruments) or Reference 600 potentiostat (Gamry Instruments). A three-electrode Teflon beaker cell comprised pristine Si (100), Si(100)/Cu, Si(100)/PPy or Si(100)/Cu/PPy working electrode and Li-foil counter and reference electrodes [17]. Only front center area of 0.33 cm^2 of the working electrode was exposed to the electrolyte. The edges and the backside of the wafer were sealed off from contact with the electrolyte. The CV cutoff voltages were set at 2.0 and 0.005 V for the Si(100) electrodes and 2.5 and 0.005 V for the Si(100)/Cu electrodes. All potentials reported in this work are referenced vs. Li/Li$^+$ electrode. After CV measurements, the working electrode was rinsed with DMC for 30 s and dried in the glove box prior to spectroscopic and microscopic analysis. All electrochemical measurements were performed inside a glove box filled with He gas (H$_2$O and O$_2$ content < 1 ppm).

2.4. Binder adhesion measurements

Adhesion force measurements were carried out on polymer-coated Si(100) or Si(100)/Cu samples using Chatillon TCD225 series force measurement system. The adhesion test method was adopted from the previous work by Vogl et al. [18]. 10 μL of saturated solution of polymer binders in N-methyl-2-pyrrolidone (PPy and PVDF) or H$_2$O (PAALi, pH∼7) was drop casted and squeezed with a force of 10–30 N, using a Transducer Techniques (Temecula, CA) LBC-250 load cell attached to a DPM-3 monitor (same company), between two 1 cm^2 Si (100) or Si(100)/Cu wafers. The sandwiched wafers were dried following the protocol used for manufacturing of composite Si anodes [15] *i.e.*, the samples were dried overnight at room temperature and further dried at 120 °C for 15 h under vacuum. Adhesion tests after drying at room temperature only were also performed for comparison purposes. The samples were fixed horizontally in the sample holder and Scotch Magic tape was applied over the backside of the upper Si wafer and used to pull it at 1 inch min^{-1} rate until the wafers were completely separated. The force used to separate the wafers was measured and compared for different binders and drying conditions.

2.5. Surface spectroscopy of Si(100) electrodes

Ex situ attenuated total reflectance Fourier transform infrared (ATR-FTIR) spectroscopy measurements were performed for the cycled, rinsed and dried samples inside an N$_2$-filled environmental chamber (818GBB/Plaslabs). A Shimadzu IRTracer-100 spectrophotometer outfitted with single reflection PIKE technologies MIRacle™ ATR sampling accessory equipped with Ge crystal was used to record ATR-FTIR spectra. The spectra were accumulated over 200 scans with spectral resolution of 4 cm^{-1}.

The near-edge X-ray absorption fine structure (NEXAFS) experiments were performed on beamlines 6.3.1.2 and 8.0.1 at the Advanced Light Source (ALS) in Lawrence Berkeley National Laboratory. The NEXAFS spectra were recorded in total-electron-yield (TEY) mode by monitoring the sample drain current. The energy resolution was set to 0.1 eV and 0.2 eV for carbon K-edge and oxygen K-edge, respectively.

Ex situ X-ray photoelectron spectroscopy (XPS) was acquired using a Kα spectrometer (Thermo Scientific) using Al Kα radiation (hν = 1486.6 eV) under ultra-high vacuum (< 1 × 10–12 atm). The spot size, energy step, and pass energy were 400 µm, 0.05 eV, and 60 eV respectively. The electrodes were transferred from Ar-filled glovebox to the XPS chamber under vacuum, using a sealed transfer module (Thermo Scientific).

2.6. Surface imaging of Si(100) electrodes

The surface morphology of the rinsed and dried Si(100) samples after electrochemical cycling was imaged using scanning electron microscopy (SEM) (JSM-6700F, JEOL) at 5 kV. *In situ* AFM imaging was carried out with an Agilent 5500 microscope in an environmental chamber filled with Ar and housing a custom-made three-electrode electrochemical cell. The electrochemical cell was assembled inside Ar-filled glovebox (H_2O and O_2 contents < 1 ppm) and transferred to the environmental chamber for AFM imaging.

Si(100)/PPy was used as a working electrode and lithium foil served as a counter and reference electrodes. The cell was filled with electrolyte and the environmental chamber was saturated with DEC vapor to prevent the loss of electrolyte in the AFM cell. Linear sweep voltammetry (LSV) was conducted from OCP (ca. 3.2 V) to 5 mV at 0.1 mV s^{-1} scan rate and the AFM contact mode images were recorded at various potentials.

3. Results and discussion

3.1. Characterization of mechanical properties of PPy, PVdF and PAALi binders

The relative binding strength of PPy, PVdF and PAA to Si(100) and Si(100)/Cu wafers were measured at room temperature (RT) as a function of the test samples drying protocols. The chemical bonding between the binder and the Si and Cu surface and/or the tensile strength of the polymer itself can be directly correlated to the force needed to separate the Si or Cu pieces *glued* together by the binder. The results are summarized in Table 1.

The degree of adhesion and/or mechanical strength of the polymer binders vary greatly with the drying temperature. After drying at room temperature, PPy and PVdF binders showed moderately strong adhesion to Si whereas PAALi exhibited strong binding force. It has been reported that COOH groups in PAALi can participate as acceptor and

donor in hydrogen bonding with the silanol groups on Si surface [19]. Hence, the better binding of PAALi to Si(100) than PPy at room temperature can be explained by the presence of larger number of sites in PAALi for hydrogen bonding with the silanol groups. Moreover, the water-based PAALi solution may lead to the formation of fresh oxide layer on Si surface, which can promote formation of a stronger bond between PAA and SiO_2 [19]. It should be noted that the formation of a thick oxide layer would be undesirable as it may adversely affect performance of the silicon anode [11]. The ester functional groups in PPy can also acts as a hydrogen bond acceptor but the observed similar adhesion strength of PVdF and PPy to Si after drying at room temperature may also suggest other surface reaction mechanism(s). Interestingly, prolonged drying at 120 °C had no effect on the bonding strength of PPy to silicon, which remained almost the same. On the other hand, PVdF and PAALi have lost their affinity to silicon almost completely.

For Si(100)/Cu wafer samples dried at RT, PPy and PAALi exhibited strong adhesion. Interestingly, no adhesion was observed for PVdF. Drying at elevated temperature had no effect on PPy, which maintained strong adhesion to copper. Conversely to the observations on bare Si, drying at 120 °C helped PVdF and PAALi build their bonding strength to Cu. The drying process can result in the lessening of mechanical stress and increases the adhesion of the binders to the substrate [20,21]. On the other hand, the chemical composition of the surface *vs.* reactivity of the binder can facilitate or inhibit creation of chemical bonds and affect the strength of the adhesion [20].

These results demonstrate that PPy exhibits better bonding properties to Si(100) and Si(100)/Cu wafers than PVdF and PAALi, independent of the drying protocol. Most likely, the strong interaction between the PPy and silicon and copper native oxides results in formation of strong covalent bonding between methyl methacrylate ester groups on PPy and the hydroxide-terminated SiO_2 surface via a *trans*-esterification reaction [22]. This chemical coordination bond is much stronger than the hydrogen bonding between SiO_2 or CuO and PAALi or PVdF [23]. These observations would also explain the superior performance of the PPy binder in Si(100) composite electrodes reported by Park et al. [15].

3.2. Electrochemical measurements

Fig. 1 shows CVs of the Si(100) and Si(100)/PPy electrodes in 1 M LiPF$_6$/EC:DEC:FEC (2.1:4.9:3.0 v/v) electrolyte. For the sake of clarity, the inset in the CV plot of the pristine Si(100) wafer electrode (Fig. 1a) shows a magnified view of the cathodic current in the electrolyte reduction potential region. The uncoated Si(100) electrode shows four cathodic and two anodic peaks during the first cycle. The onset potential of the electrolyte reduction was observed at 2.25 V, consistent with the previous study for FEC containing electrolyte [17]. The shoulder at 1.3 V, and the sharp feature at 0.8 V correspond to the decomposition of DEC and EC, respectively [24]. A small feature due to the initial lithiation of crystalline Si(100) at 0.2 V is followed by a steep increase of the cathodic current and lithiation of silicon at 0.11 V. The anodic peaks at 0.32 V and 0.52 V correspond to the delithiation process [25].

During the 2nd cycle the cathodic peaks at 1.3 and 0.8 V are suppressed, whereas the small peak at 0.38 V, which has shifted from 0.5 V is still present, indicating partial passivation of the Si(100) surface. Also, the onset potential of the lithiation of Si on the 2nd and following cycles shifted to 0.6 V, which was accompanied by a similar anodic shift of the delithiation peaks which eventually fused into a single feature after 8th cycle.

The CVs of the Si(100)/PPy electrode exhibit a radically different electrochemical behavior from the uncoated Si(100) electrode (Fig. 1b). In the 1st cycle, similar cathodic features are observed, but the original peaks at 1.3 and 0.38 V appear shifted to 1.1 and 0.2 V, respectively. No obvious features that can be ascribed to reduction of PPy were
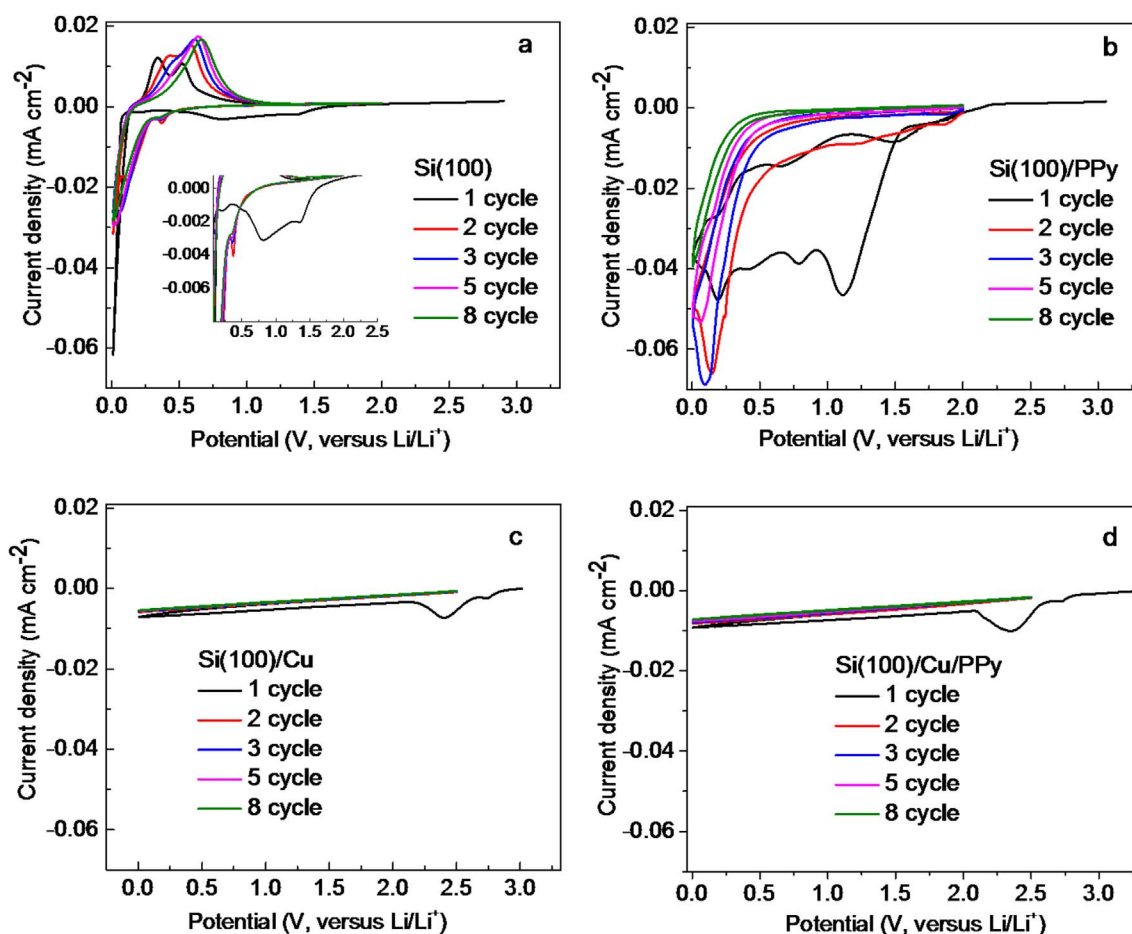
Table 1
Adhesion tests of PPy, PAALi and PVdF to Si(100) and Si(100)/Cu wafers after drying at RT and 120°C in vacuum. *The units are given in newton (N). ** and *** The force used to separate the wafers was too high or too low, respectively, and could not be recorded by the instrument.

Si(100) wafers*(N)			Si(100)/Cu wafers*(N)	
Binder	24 h at RT	24 h at RT and 15 h at 120 °C in vacuum	24 h at RT	24 h at RT and 15 h at 120 °C in vacuum
PPy	6.94 ± 0.58	6.49 ± 0.49	**Strong adhesion	**Strong adhesion
PVdF	7.25 ± 0.22	0.19 ± 0.07	***No adhesion	**Strong adhesion
PAALi	***Strong adhesion	***No adhesion	8.72 ± 0.18	**Strong adhesion

Fig. 1. Cyclic voltammetry of (a) pristine Si(100), (b) Si(100)/PPy, (c) Si(100)/Cu and (d) Si(100)/Cu/PPy electrodes in 1.2 M LiPF$_6$/EC:DEC:FEC (2.1:4.9:3.0 v/v) at a scan rate of 0.1 mV s^{-1}.

observed. Importantly, the peak currents become much higher and their relative intensities varied significantly, indicating that the rate and possibly mechanism of the electrolyte decomposition on the Si(100)/PPy have changed considerably. The shift of the cathodic peaks to lower potentials might be attributed to electrode polarization due to charge and/or mass transport limitation in the PPy film. On the other hand, the amount of cathodic charge consumed on the Si(100)/PPy during the 1st scan between 2 V and 0.3 V (0.028 C cm^{-2}) is approximately ten times more than the uncoated Si(100) electrode. Also, the charge consumed in this region is much higher than the hypothetical charge needed for complete reduction of PPy to elemental carbon (0.012 C cm^{-2}) [13]. This indicates the increased interfacial reactivity in the presence of PPy, which is also exacerbated by considerably high cathodic current during the 2nd and following scans, especially for the peak at 0.14 V. Interestingly, the total absence of delithiation anodic peaks implies that lithiation process was seriously inhibited during the cathodic scan and all the observed electrochemical activity originates from the electrolyte and possibly PPy decomposition reactions.

To investigate electrochemical stability of PPy, the Si(100)/Cu and Si(100)/Cu/PPy electrodes were cycled under similar conditions (Fig. 1c and d). The CV of the Si(100)/Cu electrode shows a peak at 2.3 V attributed to the reduction of surface oxygen impurities [26] and no cathodic current due to the decomposition of electrolyte is observed as the potential was scanned to 0.005 V. The CV of Si(100)/Cu/PPy exhibits a similar feature at 2.3 V with Cu and no cathodic peaks that can be ascribed to the electrolyte or PPy reduction, indicating electrochemical stability and no reactivity of PPy toward the electrolyte within the potential operation range of the Si anode.

3.3. Ex situ surface analysis of the cycled Si(100) and Si(100)/PPy electrodes

To further study the chemical stability of PPy, the PPy powder was soaked in the electrolyte for 24 h, filtered, washed with DMC and dried for 24 h in the glovebox. FTIR and TGA analysis of the pristine and electrolyte-treated PPy powder were carried out (Fig. 2). All IR spectral characteristic features of the pristine PPy powder are also observed for the PPy exposed to the electrolyte, indicating no chemical degradation of PPy in the electrolyte. However, the presence of additional peaks at 1775 and 1810 cm^{-1} in the FTIR spectrum of the electrolyte-treated PPy powder are attributed to the electrolyte solvents, which are trapped in the PPy structure.

The TGA profile of the electrolyte-treated PPy shows an initial 17% weight loss prior to decomposition of PPy, which is absent in the pristine PPy powder. Considering much lower boiling temperature of DEC (127 °C) than FEC (212 °C) or EC (243 °C) and consequently much higher heat release rate of DEC than FEC and EC [27], the observed weight loss can be attributed predominantly to evaporation of DEC at T < 170 °C and FEC/EC at T < 310 °C trapped in the PPy. Considering the original solvent composition of the electrolyte EC:DEC:FEC (2.1:4.9:3.0 v/v and the observed 13% mass loss at T < 170 °C vs. only 4% between 170 °C < T < 310 °C one may conclude that DEC has been preferentially absorbed by PPy powder during soaking in the electrolyte.

Fig. 3a shows *ex situ* FTIR spectra of the pristine Si(100)/Cu/PPy and cycled Si(100)/Cu and Si(100)/Cu/PPy electrodes. The spectrum of the pristine Si(100)/Cu/PPy is almost identical to the cycled electrode and dominated by the spectral features of PPy. This observation further
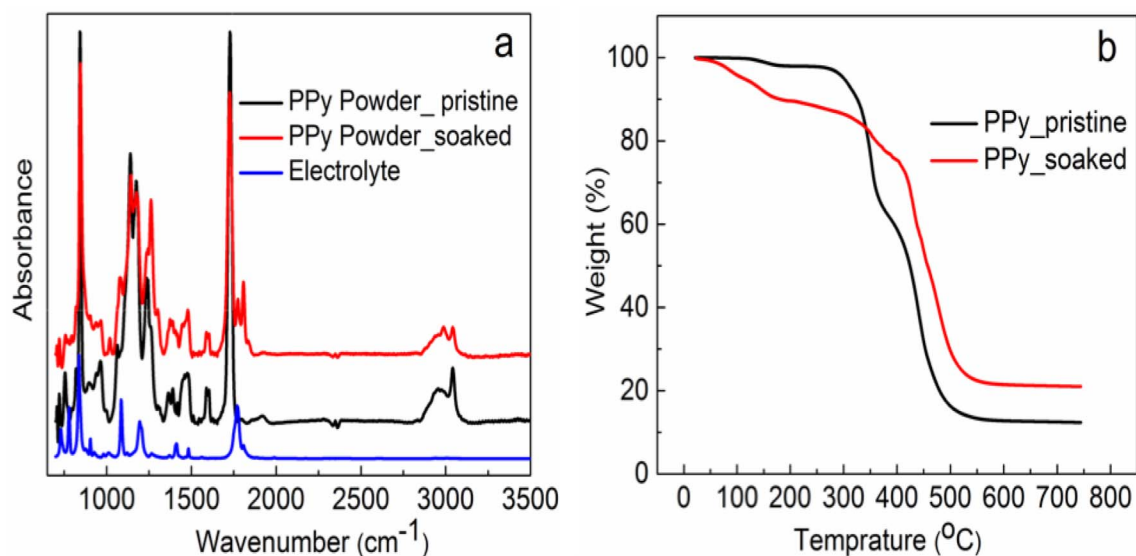
Fig. 2. (a) FTIR of the electrolyte and PPy powder before and after soaking in the electrolyte and drying at RT for 24 hours, (b) TGA profiles of the pristine PPy powder and after soaking in the electrolyte and drying at RT for 24 hours.

confirms the (electro)chemical stability of PPy, which is consistent with the electrochemical data. The spectrum of the cycled Si(100)/Cu shows some weak features from the electrolyte reduction products but these peaks are obscured (except the peak at 1300 cm^{-1}) by PPy IR bands in the cycled Si(100)/Cu/PPy electrode.

The FTIR spectra of the Si(100) and Si(100)/PPy electrodes after 8 cycles are shown in Fig. 3b. These results reveal different spectral characteristics (denoted by * in Fig. 3b) and changes in the relative peak ratios evidently indicating variations of chemical composition in the corresponding surface films. Though the peak distribution pattern of the Si(100) and Si(100)/PPy electrodes below 1300 cm^{-1} is comparable, the different FTIR peak intensities and ratios indicate variations of thickness and chemical composition of the surface films on the cycled Si(100) and Si(100)/PPy electrodes. In the FTIR spectrum of the cycled Si(100)/PPy, the intense peaks at 2850 and 2930 cm^{-1} due to the asymmetric C-H stretching, the shoulder at 1020 and the peak at

778 cm^{-1} due to asymmetric Si-O stretching, and the peak at 1160 cm^{-1} due to O-C stretching of Si-O-CH$_3$ group shows the presence of Si containing reduction reaction products [24,28]. Moreover, the FTIR peaks of the cycled Si(100)/PPy in the region from 1300 to 1750 cm^{-1} is different from the Si(100) electrode suggesting the variation of the film formation process at the electrode/electrolyte interface. Contrary to the cycled Si(100)/Cu/PPy electrode the PPy peaks could not be seen in the spectrum of the cycled Si(100)/PPy most likely because of the thick overlayer of the electrolyte decomposition products.

To investigate surface morphology changes of the PPy film during cycling a series of AFM measurements were carried out. *In-situ* AFM images of the pristine Si(100)/PPy electrode and after soaking in the electrolyte at open circuit voltage (OCV) (ca. 3.2 V) for 30 min are shown in Fig. 4a and 4b, respectively. For ease of comparison, the same depth color contrast scale that corresponds to 0–15 nm is used. The
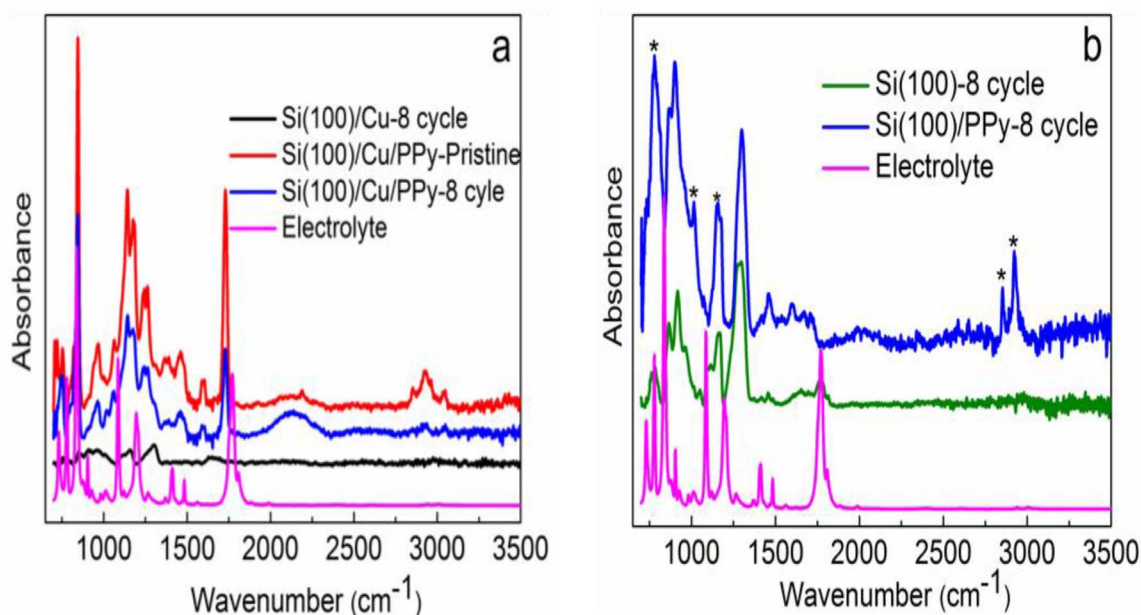

Fig. 3. *Ex situ* FTIR spectra of (a) pristine Si(100)/Cu/PPy and cycled Si(100)/Cu and Si(100)/Cu/PPy electrodes, and (b) Si(100) and Si(100)/PPy cycled electrodes. FTIR spectrum of the electrolyte is also included for reference.
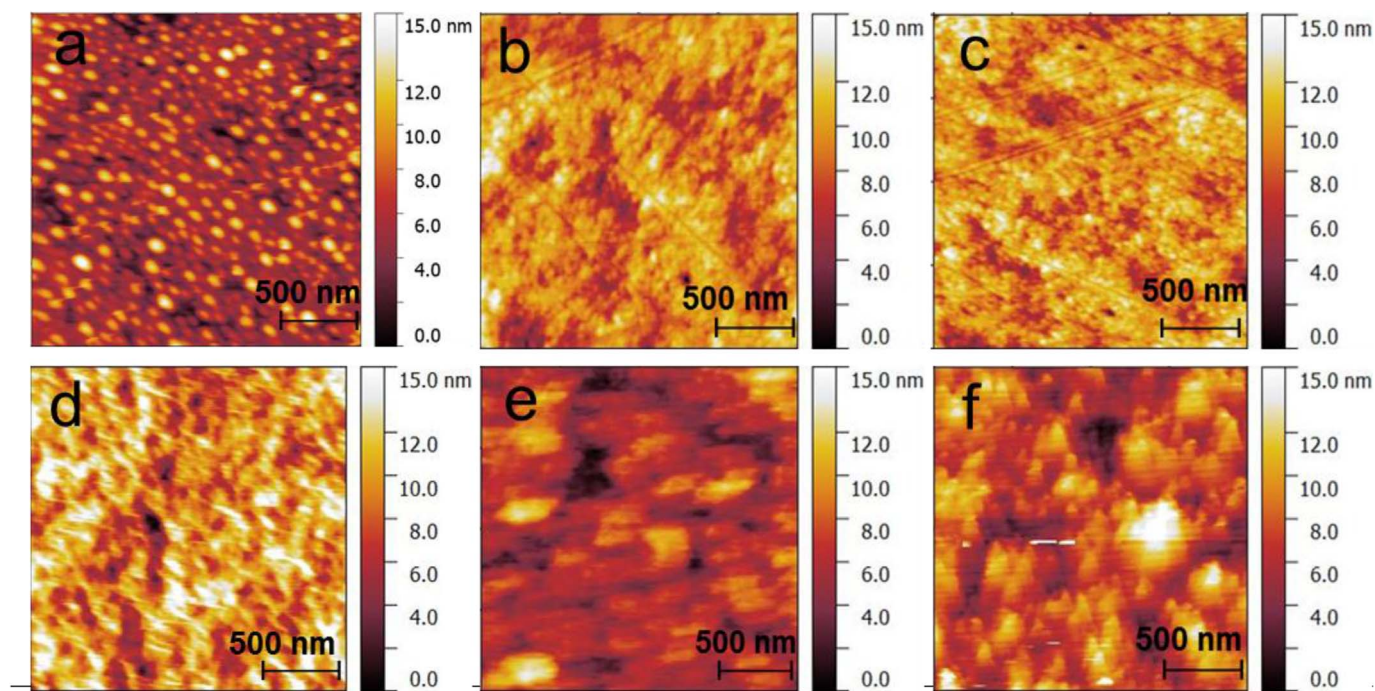
Fig. 4. *In situ* AFM 2.0 x 2.0 μm images of the Si(100)/PPy electrode (a) pristine, (b) exposed to the electrolyte at OCV (3.2 V) for 30 min, (c) at 3.1 V, (d) 2.25 V, (e) 1 V, and (f) at 0.005 V.

AFM image of the pristine PPy film shows a uniform and compact matrix of spherical particles with size ranging from 50 to 100 nm. A notable change of the surface morphology due to electrolyte uptake was observed after the Si(100)/PPy electrode was exposed to the electrolyte. The particles tend to form aggregates of irregular sizes and shapes, which may relate to possible swelling of the polymer. The root mean square (RMS) roughness of the electrode increases slightly from 1.9 to 2.2 nm for 2 × 2 μm. In a separate measurement, the Si(100)PPy electrode was scratched and AFM profile was recorded before and after soaking in the electrolyte for 30 min. The depth profiling measurements show that the PPy film swells by ~18% upon exposure to the electrolyte.

In-situ AFM images of the Si(100)/PPy electrode during the first cathodic scan are shown in Fig. 4c–f. As the electrode potential was scanned from OCV (ca. 3.2 V) to 0.005 V, significant changes in the surface morphology of the electrode are observed. At the onset potential of electrolyte decomposition (2.25 V) the RMS roughness increases to 2.65 nm and electrolyte decomposition products on top of the PPy film become more clearly observable. The RMS roughness does not change significantly as the potential further decreases to 0.005 V, but the surface morphology, size and shape of surface feature, changes quite dramatically as the electrolyte reduction process goes through different stages as depicted in the corresponding CV (Fig. 1b).

Ex-situ SEM images of the Si(100) and Si(100)/PPy electrodes after 8 cycles are shown in Fig. 5. The pristine silicon (Fig. 5a) and silicon coated with PPy (Fig. 5d) appear largely featureless on the SEM micrographs as one may expect. However, upon cycling of the pristine Si (100) electrode (Fig. 5b and c), the topography of the anode surface appears rough and highly inhomogeneous, and consists of coarse surface features, attributed to the formation or agglomeration of the electrolyte reduction products of various sizes and morphology. On the other hand, the surface film on the cycled Si(100)/PPy electrode is comparatively uniform, consisting of densely packed particles. These differences in surface morphology between the cycled Si(100) and Si (100)/PPy electrodes again point towards variations of the surface film formation process, which is consistent with the CV, and FTIR results described previously.

Fig. 6a shows the C K-edge NEXAFS spectra of the pristine and cycled Si(100) and Si(100)/PPy electrodes. The spectra of the pristine Si (100)/PPy and cycled Si(100) and Si(100)/PPy electrodes after 2 or 8 cycles show the typical π* features of C=C, C-O and C=O bonds. The feature at ~293 eV corresponds to 1s → σ* transitions of C=C bonds. For the O K-edge spectra, the feature at ~537.5 eV is assigned to the σ* states of C-O bonds. The spectrum of the Si(100) electrode after 2 cycles shows a broad feature at ~285.5 eV, which could originate from the electrolyte reduction products. These results support the outcome of the FTIR analysis that the PPy film remains stable at the Si and Cu surface during cycling. On the other hand, the observed slight changes in the C=C, C-O and C=O peaks relative intensities could indicate variations in the chemical composition and/or distribution of the electrolyte reduction products on the Si(100) and Si(100)/PPy.

The stability of PPy is also confirmed by the O K-edge NEXAFS spectra, as shown in Fig. 6b. The spectra of the pristine Si(100)/PPy electrode and after 2 or 8 cycles show similar π* features of C=O and C-O bonds at ~533 eV and ~535.5 eV, respectively, and σ* features of C-O bonds of PPy at ~540 eV, which again suggested at the electrochemical stability of the PPy coating on Si surface.

XPS spectra for the Si(100) and Si(100)/PPy electrodes before and after 8 cycles are provided in Fig. 7. Before cycling (the 1st row), the pure Si peak at 99.4 eV is clearly observed for the pristine Si(100) electrode (Fig. 7c). There is also a broad peak at 103.4 eV consistent with the presence of a low concentration of Si-O. The O 1s spectra of the pristine Si(100) electrode contains the corresponding Si-O peak at 532.5 eV. The C 1s spectrum contains a single peak at 285 eV characteristic of C-H, which can be assigned to the universal carbon contamination and organic impurities on the surface of the silicon. Upon coating the Si(100) with the PPy polymer, there is no observable peak in the Si 2p spectra consistent with the PPy polymer completely covering the Si surface. The PPy coating is composed primarily of carbon (Fig. 7a) and oxygen (Fig. 7b) containing species. In addition to the peak characteristic of C-H, a small peak characteristic of CO_2 (289 eV) is observed in the C 1s spectra.

After 8 cycles, surface films are generated on the surfaces of both electrodes. On the Si(100) surface (the 2nd row), the C 1s spectrum
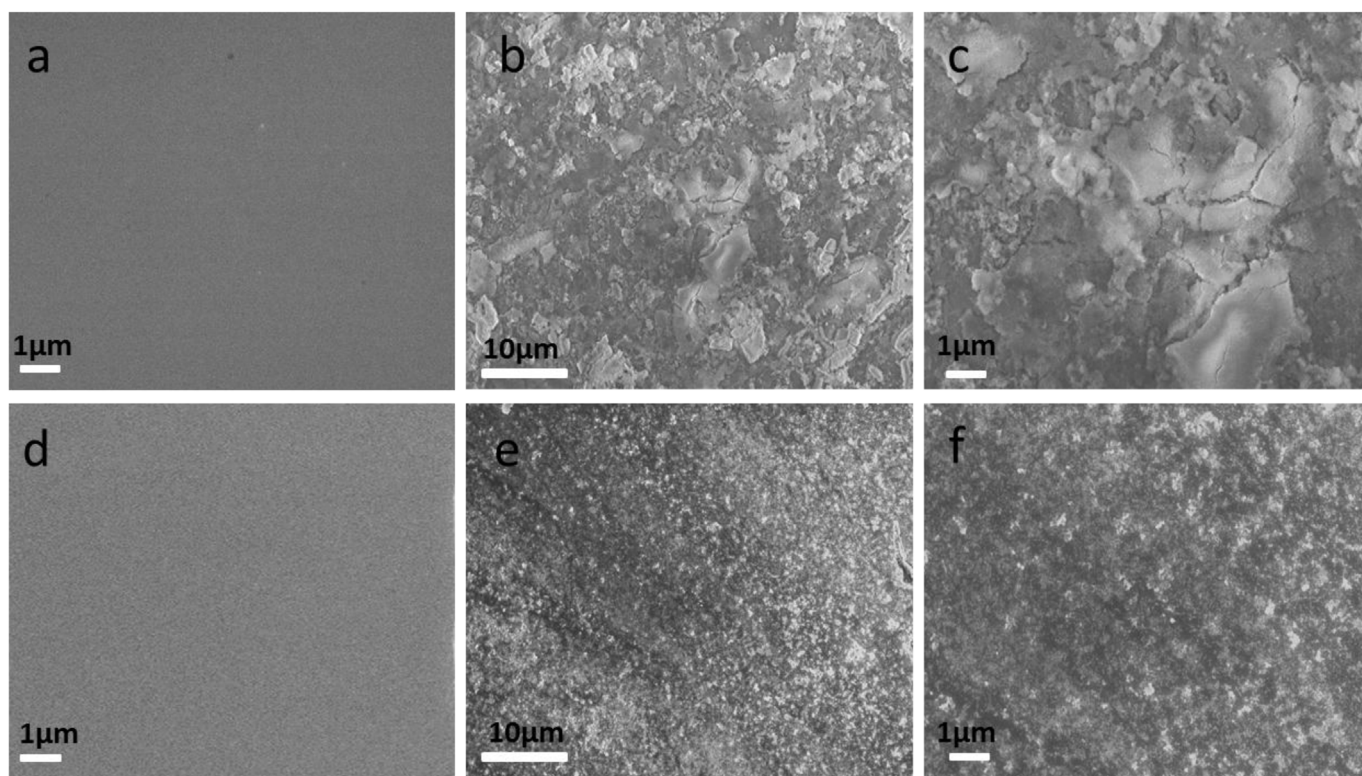
Fig. 5. SEM image of (a) pristine Si(100), (b) and (c) Si(100) after 8 cycle, (d) pristine Si(100)/PPy, (e) and (f) Si(100)/PPy after 8 cycles.
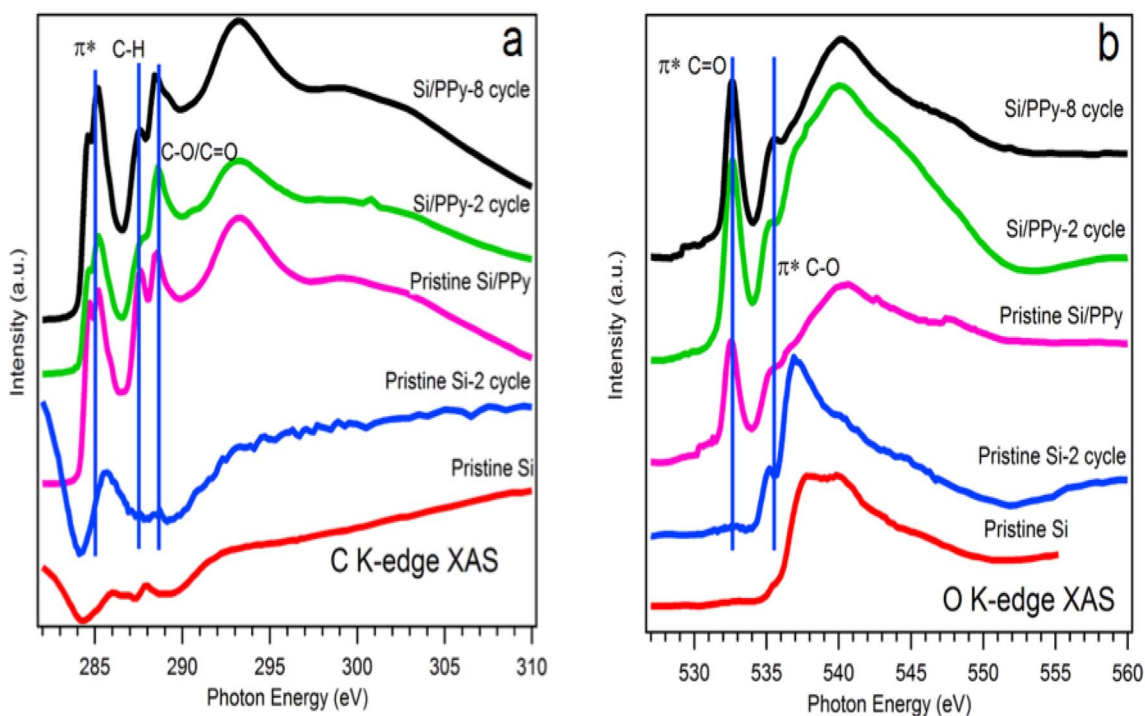

Fig. 6. (a) C K-edge and (b) O K-edge NEXAFS spectra of the pristine and cycled Si(100) and Si(100)/PPy electrodes.

contains the C-H peak along with a small new peak at 283 eV which may be due to the presence of C-Si species (Fig. 7d). The Si 2p spectrum is dominated by the peak of pure Si while the peak characteristic of Si-O is diminished (Fig. 7f). Overall, the film composition does not change significantly upon Ar^+ sputtering even for extended times (e.g. 960s), except for a slight decrease in the C 1s signal.

The surface of the Si(100)/PPy is also significantly modified after 8

cycles (the 3rd row). The C1s spectrum at topmost is similar to that of uncycled Si(100)/PPy electrode which contains peaks at 285 and 289 eV, characteristic of C-H and CO_2 containing species (Fig. 7g). Upon Ar^+ sputtering, these two peaks are relatively decreased, while the peak around 286.8 eV is relatively increased. The peak at 286.8 is characteristic of C-O. The O1s spectrum (Fig. 7h) changes significantly upon cycling with an increase in a broad peak centered at ∼532 eV
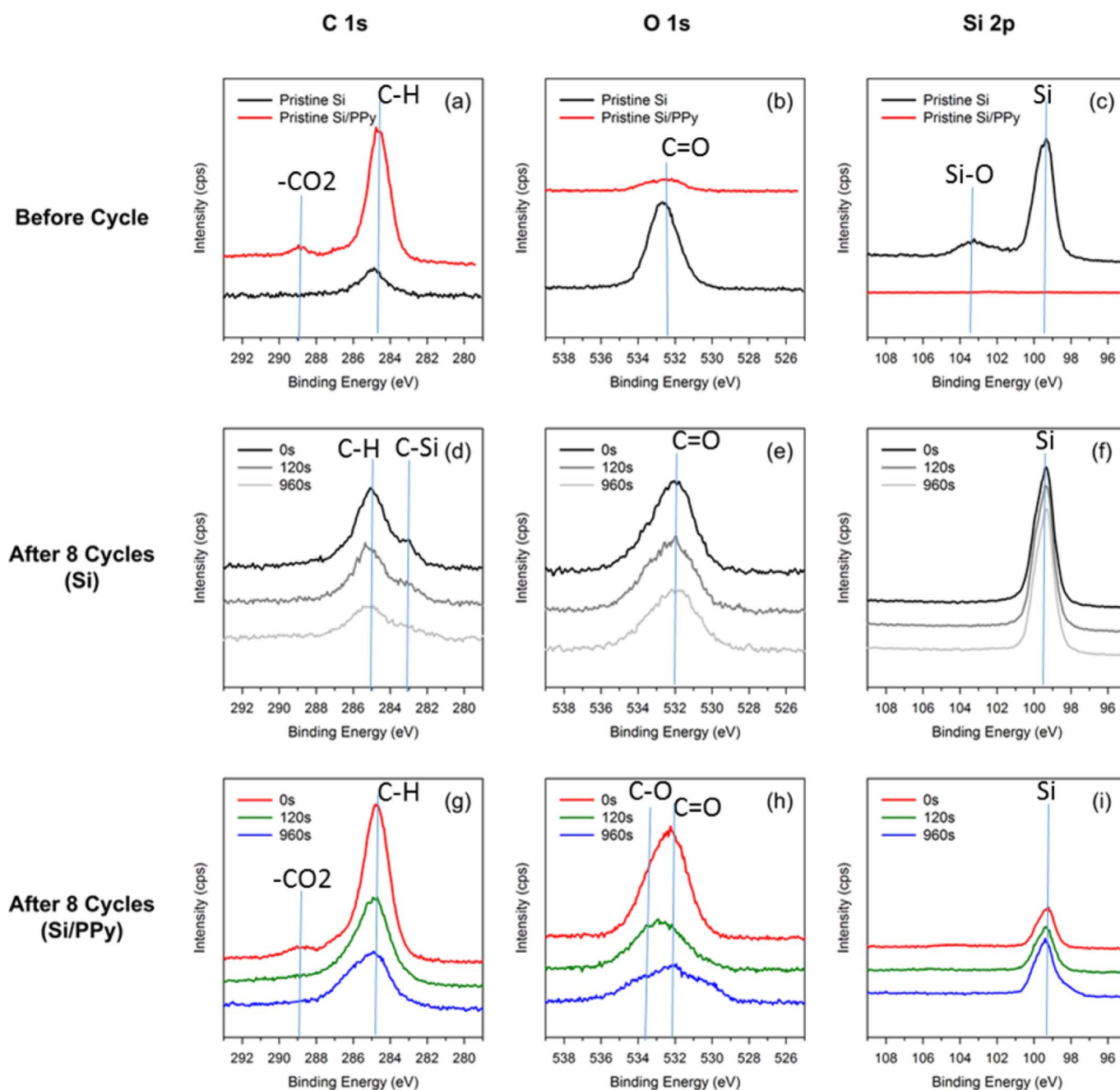
Fig. 7. XPS spectra for the Si(100) and Si(100)/PPy electrodes before (the upper row) and after 8 cycles (the lower row).

characteristic of a mixture of C-O and C=O contain species characteristic of the decomposition products of the carbonate solvents [29]. This broad peak is decreased upon Ar$^+$ sputtering, consistent with the changes observed in the C1s spectra, and a new broad peak appears at 530.5 eV, which may be consistent with LiOH. The changes upon sputtering suggest that the surface film on Si(100)/PPy has a more complex structure composed of organic species. This is consistent with the conclusion that the PPy film is still intact after cycling. Interestingly, the pure Si peak is observed on the Si(100)/PPy electrode after 8 cycles (Fig. 7i), although the signal is weaker than that observed on the cycled Si(100) electrode.

We attribute the observed differences in electrochemical response of the Si(100) and Si(100)/PPy electrodes to the preferential absorption of DEC into the PPy film because of its lower viscosity and higher mobility compared to EC or FEC. The faster transport and increased concentration of DEC in the PPy film and at the Si surface leads to the formation

of soluble products that tend to diffuse through the PPy layer and dissolve in the electrolyte [25]. In other words, the silicon surface in the Si (100)/PPy electrode most likely interacts with the electrolyte of different composition *i.e.*, enriched in DEC than the bulk composition. This leads to excessive electrolyte decomposition and poor passivating behavior.

This is also consistent with the observed inhibition of the Li$^+$ transport through the PPy layer. Li$^+$ ions in mixed organic electrolytes such as EC + DEC are solvated mainly with EC because of its high polarity and slightly higher donor number (EC = 16.4, DEC = 16) [30]. Matsuda et al. have reported that though small participation of DEC in solvation was observed, Li-ions solvated preferentially to EC, and main solvated species were Li (EC)$^{2+}$ [31]. Because EC diffusion through the PPy film is greatly inhibited, transport of EC-solvated Li$^+$ ions can be also impeded even to a larger extent.

4. Summary and conclusions

The observed fundamental chemical and physical properties of the PPy polymer is highly relevant to its use as a binder specifically for Si anodes in Li-ion batteries. On one hand, PPy shows superior adhesion toward Si and suggesting that PPy can improve mechanical integrity and stability of Si composite electrodes as compared to conventional binders such as PVdF. The microscopic and spectroscopic of the cycled Si(100)/PPy and Si(100)/Cu/PPy electrodes demonstrate that PPy binder is chemically stable in conventional Li-ion organic carbonate electrolyte and electrochemically stable within the operational potential range of the Si anode. However, the presence of the PPy film on the Si(100) surface alters the rate and possibly the mechanism of passive film formation. The Si(100)/PPy electrode exhibits excessive electrolyte reduction during initial CV cycles and inhibits Li^+ transport through the PPy film preventing lithiation of the underlying Si. The induced electronic conductivity of the PPy may exacerbate the electrolyte reduction reactions relative to the uncoated surface although this did not occur with the coated Cu electrode. It appears rather that the PPy film alters the interfacial chemistry of the Si electrode by highly selective transport of DEC relative to EC or FEC, and consequently changes the distribution of the electrolyte decomposition products toward more soluble species, which do not effectively passivate the Si surface. If the binder is applied in an optimal manner, the adverse characteristics of the binder can be avoided. The binder should not entirely coat the Si particles and only an optimum amount of the binder needed to maintain the mechanical integrity of the Si particles should be used.

In summary, the observed differences in electrochemical behavior of the model Si(100) and Si(100)/PPy electrodes demonstrate that binder (s) are not only essential to ensuring the mechanical integrity of the electrolyte but also they can alter significantly interfacial chemistry of composite electrodes by possible creation of electronic and mass transport barriers at the surface of the active material [11]. Not only the binder distribution in the composite electrode must be uniform but also the topology of the active material – binder – current collector architecture need to be carefully designed and optimized to achieve desired mechanical properties as well as stable interfacial behavior during long-term cycling.

Acknowledgment

References

[1] I.H. Son, J. Hwan Park, S. Kwon, S. Park, M.H. Rümmeli, A. Bachmatiuk, H.J. Song, J. Ku, J.W. Choi, J.-m. Choi, S.-G. Doo, H. Chang, Nat. Commun. 6 (2015) 7393.
[2] K. Ozawa, Solid State Ionics 69 (1994) 212–221.
[3] J.R. Szczech, S. Jin, Energy Environ. Sci. 4 (2011) 56–72.
[4] C.K. Chan, H. Peng, G. Liu, K. McIlwrath, X.F. Zhang, R.A. Huggins, Y. Cui, Nat. Nanotechnol. 3 (2008) 31–35.
[5] B. Philippe, R. Dedryvère, J. Allouche, F. Lindgren, M. Gorgoi, H. Rensmo, D. Gonbeau, K. Edström, Chem. Mater. 24 (2012) 1107–1115.
[6] A. Tokranov, R. Kumar, C. Li, S. Minne, X. Xiao, B.W. Sheldon, Adv. Energy Mater. 6 (2016).
[7] H. Buqa, M. Holzapfel, F. Krumeich, C. Veit, P. Novák, J. Power Sources 161 (2006) 617–622.
[8] D. Mazouzi, Z. Karkar, C. Reale Hernandez, P. Jimenez Manero, D. Guyomard, L. Roué, B. Lestriez, J. Power Sources 280 (2015) 533–549.
[9] J. Li, R.B. Lewis, J.R. Dahn, Electrochem. Solid-State Lett. 10 (2007) A17–A20.
[10] A. Magasinski, B. Zdyrko, I. Kovalenko, B. Hertzberg, R. Burtovyy, C.F. Huebner, T.F. Fuller, I. Luzinov, G. Yushin, ACS Appl. Mater. Interfaces 2 (2010) 3004–3010.
[11] C.C. Nguyen, T. Yoon, D.M. Seo, P. Guduru, B.L. Lucht, ACS Appl. Mater. Interfaces 8 (2016) 12211–12220.
[12] M. Ling, M. Liu, T. Zheng, T. Zhang, G. Liu, J. Electrochem. Soc. 164 (2017) A545–A548.
[13] B.N. Wilkes, Z.L. Brown, L.J. Krause, M. Triemert, M.N. Obrovac, J. J. Electrochem. Soc. 163 (2016) A364–A372.
[14] H. Wu, G. Yu, L. Pan, N. Liu, M.T. McDowell, Z. Bao, Y. Cui, Nat. Commun. 4 (2013) 1943.
[15] S.-J. Park, H. Zhao, G. Ai, C. Wang, X. Song, N. Yuca, V.S. Battaglia, W. Yang, G. Liu, J. Am. Chem. Soc. 137 (2015) 2565–2571.
[16] G. Liu, S. Xun, N. Vukmirovic, X. Song, P. Olalde-Velasco, H. Zheng, V.S. Battaglia, L. Wang, W. Yang, Adv. Mater. 23 (2011) 4679–4683.
[17] U.S. Vogl, S.F. Lux, E.J. Crumlin, Z. Liu, L. Terborg, M. Winter, R. Kostecki, J. Electrochem. Soc. 162 (2015) A603–A607.
[18] U.S. Vogl, P.K. Das, A.Z. Weber, M. Winter, R. Kostecki, S.F. Lux, Langmuir 30 (2014) 10299–10307.
[19] S.-L. Chou, Y. Pan, J.-Z. Wang, H.-K. Liu, S.-X. Dou, Phys. Chem. Chem. Phys. 16 (2014) 20347–20359.
[20] K. Kierzek, J. Mater. Eng. Perform. 25 (2016) 2326–2330.
[21] S. Lim, S. Kim, K.H. Ahn, S.J. Lee, Ind. Eng. Chem. Res. 54 (2015) 6146–6155.
[22] H. Zhao, Z. Wang, P. Lu, M. Jiang, F. Shi, X. Song, Z. Zheng, X. Zhou, Y. Fu, G. Abdelbast, X. Xiao, Z. Liu, V.S. Battaglia, K. Zaghib, G. Liu, Nano Lett. 14 (2014) 6704–6710.
[23] H. Huang, G. Han, J. Xie, Q. Zhang, Int. J. Electrochem. Sci. 11 (2016) 8697–8708.
[24] Y. Horowitz, H.-L. Han, P.N. Ross, G.A. Somorjai, J. Am. Chem. Soc. 138 (2016) 726–729.
[25] F. Shi, Z. Song, P.N. Ross, G.A. Somorjai, R.O. Ritchie, K. Komvopoulos, Nat. Commun. 7 (2016) 11886.
[26] D. Aurbach, M. Daroux, P. Faguy, E. Yeager, J. Electroanal. Chem. 297 (1991) 225–244.
[27] G.G. Eshetu, S. Grugeon, S. Laruelle, S. Boyanov, A. Lecocq, J.-P. Bertrand, G. Marlair, Phys. Chem. Chem. Phys. 15 (2013) 9145–9155.
[28] D.J. Michalak, S.R. Amy, A. Estève, Y.J. Chabal, J. Phys. Chem. C 112 (2008) 11907–11919.
[29] M. Nie, D.P. Abraham, Y. Chen, A. Bose, B.L. Lucht, J. Phys. Chem. C 117 (2013) 13403–13412.
[30] S.-I. Lee, U.-H. Jung, Y.-S. Kim, M.-H. Kim, D.-J. Ahn, H.-S. Chun, Korean J. Chem. Eng. 19 (2002) 638–644.
[31] Y. Matsuda, T. Fukushima, H. Hashimoto, R. Arakawa, J. Electrochem. Soc. 149 (2002) A1045–A1048.